Chemical Science

RSC Publishing

EDGE ARTICLE

View Article Online
View Journal | View Issue

Cite this: *Chem. Sci.*, 2013, **4**, 4285

Photophysical and theoretical investigations of the [8]cycloparaphenylene radical cation and its charge-resonance dimer†

Matthew R. Golder,[a] Bryan M. Wong[b] and Ramesh Jasti*[a]

Received 3rd July 2013
Accepted 19th August 2013

DOI: 10.1039/c3sc51861b

www.rsc.org/chemicalscience

Treatment of [8]cycloparaphenylene (CPP) with the oxidant triethyloxonium hexachloroantimonate afforded an isolable radical cation of the parent carbon nanohoop. The photophysical properties of [8]CPP$^{+}SbCl_6^{-}$ were investigated, showing the presence of two absorptions at 535 nm and 1115 nm. Time-dependent density functional theory (DFT) calculations were used to examine these optical absorptions, revealing a delocalized, quinoidal carbon nanohoop. Upon mixing with neutral [8]cycloparaphenylene, the formation of an unusually strong charge-resonance complex $([8]CPP_2)^{+}$ was observed. Spectroscopic and computational studies were indicative of extensive intermolecular charge delocalization between the two carbon nanohoops as well.

Introduction

Understanding intramolecular[1] and intermolecular[2] charge transfer phenomena in π-conjugated materials is important for the design of better performing organic electronic materials and photovoltaics.[3–5] Small molecule aromatic radical cations can serve as excellent model systems for charge transfer processes in more complex p-type materials.[6–9] Seminal work by the groups of Kochi[10,11] and Rathore[12–15] has allowed the isolation and characterization of a variety of electron-rich aromatic radical cation salts. Unequivocal analyses of these compounds in the solid state and in solution has allowed direct structural and electronic comparisons between the charged compounds and the neutral parent compounds, providing insight into the behavior of polyphenylene materials. Furthermore, open-shell fragments of conducting polymers such as tetrathiafulvalene[16–19] and oligothiophene[20–23] have been studied as p-doped models of conducting polymers.

Radicals derived from polycyclic aromatic hydrocarbons (PAHs) are of particular importance due to their structural similarities to carbon materials such as graphene, fullerenes and carbon nanotubes (CNTs) (Fig. 1).[24,25] Numerous charged and uncharged radical planar polycyclic aromatic hydrocarbon compounds have been extensively studied,[1,25,26] suggesting varying amounts of charge delocalization throughout the respective π-systems. Additionally, studies of *in situ* generated corannulene radical cations and anions have provided insight into the structural and electronic properties of a bent PAH with unpaired electrons.[24,27–29] Although these systems were observed spectroscopically, it was not until recently that highly distorted, open-shell aromatic compounds were isolated by chemists.[30–32] These nonplanar compounds have been shown to have intriguing electronic and structural properties owing to their non-planar π-systems with three-dimensional spin delocalization.

Over the past several years, our group,[33,34] as well as the groups of Itami[35,36] Yamago,[37,38] Isobe,[39] and Müllen[40] have developed syntheses of short, neutral [*n*,*n*] armchair CNT

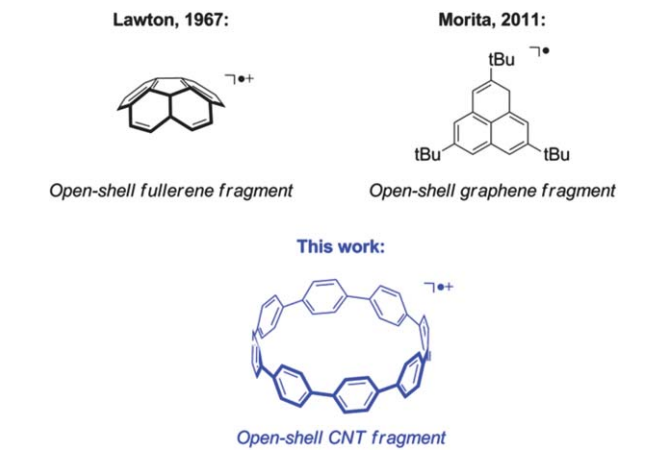

Fig. 1 The [*n*]cycloparaphenylene radical cation represents a rare example of a distorted, open-shell graphitic material.

[a]*Department of Chemistry and Division of Materials Science & Engineering and Center for Nanoscience and Nanotechnology, 24 Cummington Street, Boston, MA, USA. E-mail: jasti@bu.edu; Tel: +1 6173585543*

[b]*Department of Chemistry and Department of Materials Science & Engineering, Drexel University, 3141 Chestnut St., Philadelphia, PA 19104, USA*

† Electronic supplementary information (ESI) available: Experimental procedures, electrochemical data, photophysical data, details of Benesi–Hildebrand studies, EPR spectra and computational details. See DOI: 10.1039/c3sc51861b

fragments. These segments, [*n*]cycloparaphenylenes ([*n*]CPPs),[41–43] have attracted ample interest due to their radially-oriented π-systems, tunable optical properties and supramolecular capabilities.[34,44] With our group's ability to access carbon nanohoops[45] on the gram-scale,[34] the study of their reactivity has become increasingly viable. For example, in a recent collaboration with the Petrukhina group we have reported on the multi-electron reduction of [8]CPP to a tetraanion, an extremely distorted structure in the solid-state.[46] Herein, we report the first synthesis, theoretical analysis and photophysical characterization of quinoidal [8]CPP$^{+}SbCl_6^{-}$,[47] as well as the formation of the corresponding unusually strong charge-resonance complex, $([8]CPP_2)^{+}$.

Experimental results

Synthesis

Triethyloxonium hexachloroantimonate ($Et_3O^{+}SbCl_6^{-}$) (E_{red} = 1.5 V *vs.* SCE)[11] is a reagent that has previously been used for the generation of numerous aromatic radical cations[11,13,48] as well as the oxidation of single-walled CNTs.[8,49] Treatment of an anhydrous dichloromethane solution of [8]CPP (**1**) at 0 °C with $Et_3O^{+}SbCl_6^{-}$ immediately led to the formation of a dark orange solution that slowly became deep purple over time (Scheme 1). Upon cooling to −50 °C, the addition of anhydrous pentane led to the precipitation of a purple solid that was isolated in 67% yield. The radical cation **1**$^{+}$ was stable on the order of days at ambient temperature if excluded from excessive moisture. Additionally, exposure to zinc dust allowed its nearly quantitative reduction back to neutral [8]CPP **1**.

Structural analysis

We anticipated that EPR spectroscopy would provide insight into the electronic nature of the nanohoop radical cation **1**$^{+}$. Charge delocalization has been extensively studied *via* analysis of EPR hyperfine structures, indicating spin–orbit coupling between the unpaired electron and atoms in the π-system.[10,11,48,50–52] Unfortunately in our hands, no hyperfine structure was observed for a dilute (10^{-3} M) solution of **1**$^{+}$ in dichloromethane at 25 °C. Rather, only a single, broad line (g = 2.007) was obtained, which is consistent with the presence of a delocalized organic radical.[53] The spectrum remained unchanged upon further dilution (10^{-5} M) and cooling to below −263 °C. In addition, the spectrum remained unchanged even after the addition of 5 equivalents of oxidant (Fig. S8 in ESI†). As no EPR signal was observed for either neutral **1** or $Et_3O^{+}SbCl_6^{-}$ reagent in CH_2Cl_2, we cannot attribute the observed signal to a paramagnetic impurity introduced into the experiment (Fig. S10 in the ESI†). A number of other delocalized aromatic radical cations, such as coronene, biphenyl, phenanthrene,[1] and aza-coronene[54] portray unresolved signals as well. Additionally, attempts at characterizing **1**$^{+}$ *via* single crystal X-ray crystallography have to date been unsuccessful.[55]

Photophysical and electrochemical characterization of 1^{+}

Aromatic radical cations often have characteristic features in the near-IR (NIR) as observed in the twin absorption bands of the quaterphenyl[15] and biphenyl[56,57] radical cations. As seen in Fig. 2, **1**$^{+}$ has two major absorptions at 535 nm (ε = 0.81 (±0.03) × 10^4 M^{-1} cm^{-1}) and 1115 nm (ε = 1.03 (±0.03) × 10^4 M^{-1} cm^{-1}), which is consistent with similar aromatic radical cations. These data are in stark contrast to neutral **1**, which has an absorption at 340 nm ($\varepsilon = 1.00 \times 10^5$ M^{-1} cm^{-1}) and a broad shoulder around 400 nm.[38] The presence of the two red-shifted absorptions closely matches the values estimated by TD-DFT calculations (*vide infra*).

Spectroelectrochemical experiments (performed in 0.1 M *n*-Bu_4PF_6 in CH_2Cl_2 under ambient conditions) allowed us to monitor the formation of radical cation **1**$^{+}$ *in situ* by applying a constant potential to the sample. Use of slightly higher potentials than the sole observed $E^{ox}_{1/2}$ (0.68 V *vs.* Fc/Fc^{+}) in the cyclic voltammogram (Fig. S4 in the ESI†) led to an increase in absorption at 535 nm and a decrease in absorption at 340 nm over 10 min. An isosbestic point at 368 nm strongly supports our hypothesis that a single oxidation step occurs from neutral **1** to radical cation **1**$^{+}$ (Fig. S7 in the ESI†). This observation is consistent with the absorption in the visible region from both the chemical oxidation of neutral **1** and the calculated TD-DFT spectrum (*vide infra*). Importantly, this also provides evidence against the formation of radical cation **1**$^{+}$ *via* a disproportionation mechanism involving a dicationic species or interaction between two radical cation species to form a π-dimer.[54,58,59] Cyclic voltammetry with one equivalent of both neutral **1** and

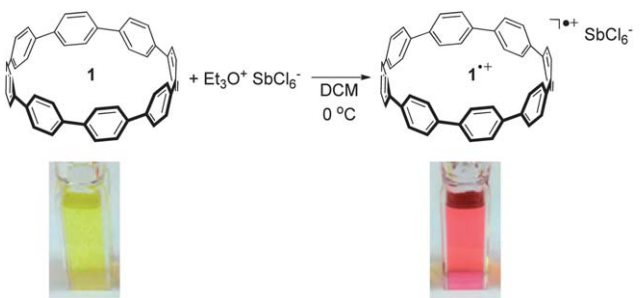

Scheme 1 Single electron oxidation of [8]CPP.

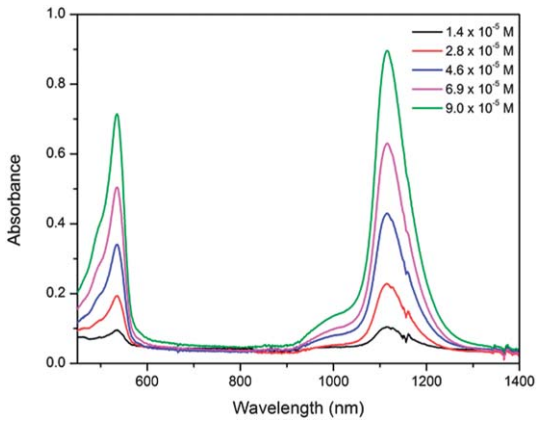

Fig. 2 UV-vis-NIR spectra of **1**$^{+}$ at increasing concentrations.

ferrocene (Fig. S5 in the ESI†) revealed almost identical integrated peak areas ($A_1/A_{Fc} = 1.06$). To further support this claim, differential pulse voltammetry experiments confirmed that the single wave observed in the cyclic voltammogram corresponds to the transfer of a single electron as evidenced by just one peak in current differential (Fig. S6 in the ESI†).[54] Lastly, evidence against a dication species is seen in the calculated TD-DFT spectrum for a $\mathbf{1}^{2+}$ species, which is inconsistent with our experimental data (Tables S6–S9 in the ESI†). These data, along with the EPR signal, absence of an absorption at 340 nm (Fig. S1 in ESI†), and nearly quantitative reduction back to neutral **1** confirm the identity and isolation of radical cation $\mathbf{1}^{+}$.

Characterization of dimer $(\mathbf{1})_2^{+}$

Charge-resonance (CR) dimers can be prepared by mixing an aromatic radical cation with its neutral counterpart, giving rise to an intense band in the NIR that results from intermolecular charge transfer. The titration of a yellow dichloromethane solution of **1** (8.2×10^{-3} M) into a purple dichloromethane solution of $\mathbf{1}^{+}$ (1.0×10^{-4} M) resulted in the formation of an orange CR dimer,[19] $(\mathbf{1})_2^{+}$. Concomitant with the gradual decrease in absorbance at 535 nm (loss of purple color) and 1115 nm was the growth of new bands at 687 nm and 1747 nm (Fig. 3). We attribute the broad absorption at 1747 nm to a CR transition that has been observed in other mixed valence dimer systems.[19,48] Specifically, this characteristic near-IR band can be ascribed to the delocalization of positive charge throughout both [8]CPP moieties. In addition, the EPR spectrum of the CR dimer $(\mathbf{1})_2^{+}$ exhibits a broad, unresolved line as well, confirming its paramagnetic character (Fig. S9 in the ESI†).

With the ability to observe the CR complex $(\mathbf{1})_2^{+}$ under ambient conditions, we next sought to investigate the dimerization process quantitatively. The Benesi–Hildebrand procedure[60] was first used to evaluate the electron transfer process between iodine and benzene[61] and later applied to mixed valence organic paramagnetic complexes.[19,48,52] Thus, we used this technique to extrapolate values for the binding constant of $(\mathbf{1})_2^{+}$, K_{dimer}, as well as the extinction coefficient of its CR band, ε_{1747}:

$$\frac{[\mathbf{1}^{\cdot+}]}{A_{1747}} = \frac{1}{\varepsilon_{1747}} + \frac{1}{K_{dimer}\varepsilon_{1747}}\frac{1}{[\mathbf{1}]} \quad (1)$$

In order to employ this procedure, we have made the assumption that **1**, $\mathbf{1}^{+}$, and $(\mathbf{1})_2^{+}$ are the only three species that exist in solution.[60] Using the data from Fig. 3 and eqn (1), a linear plot of $[(\mathbf{1})^{+}]/A_{1747}$ *vs.* $1/[\mathbf{1}]$ was constructed (Fig. 4). The slope and intercept allowed us to extract values of 1.15 (± 0.03) $\times 10^4$ M^{-1} and 2.99 (± 0.06) $\times 10^4$ M^{-1} cm^{-1} for K_{dimer} and ε_{CR}, respectively. Unexpectedly, the binding constant calculated is two orders of magnitude larger than those of charge-resonance dimers formed from octamethylbiphenylene (OMB),[48] naphthalene and pyrene.[62] "Sandwich-like" complexes from non-planar PAHs have been observed previously,[63–66] however, *a priori* one might expect planar polycyclic aromatic hydrocarbons to engage in more efficient π–π interactions than the highly distorted nanohoops. The high binding constant suggests that the interaction between the two nanohoops in $(\mathbf{1})_2^{+}$ is unusually strong compared to other known mixed valence dimers of planar aromatic systems.[67]

With a binding constant in hand, ΔG^0 for the formation of dimer $(\mathbf{1})_2^{+}$ was estimated ($\Delta G^0 = -RT \ln K_{dimer}$). By relating the change in Gibbs free energy with the equilibrium constant, K_{dimer}, we calculated that the dimerization process is exothermic by 5.55 kcal mol^{-1}. This value, however, should underestimate the true binding energy as no diffusional entropic parameters are considered for this intermolecular process. This process is in contrast to charge-transfer dimers formed by cyclophane-like radical cations where the entropic changes are negligible due to the rigidity and intramolecularity of the system.[52]

Computational analysis and discussion

Structural analysis of $\mathbf{1}^{+}$

Since we were unable to gain any detailed structural information from EPR spectroscopy and X-ray crystallographic analysis, density functional theory (DFT) calculations were performed[68]

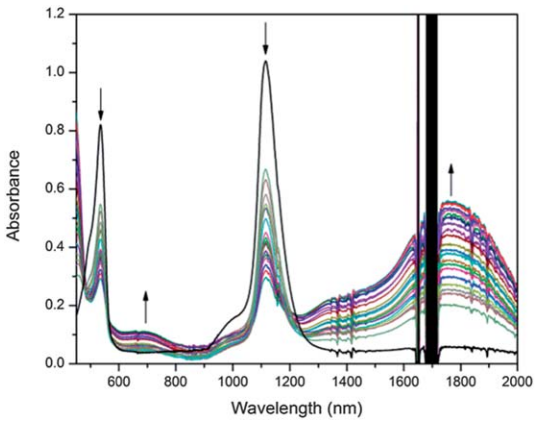

Fig. 3 Titration of neutral **1** into solution (Table S1 in the ESI†) of $\mathbf{1}^{+}$ leads to a charge-resonance band at 1747 nm.

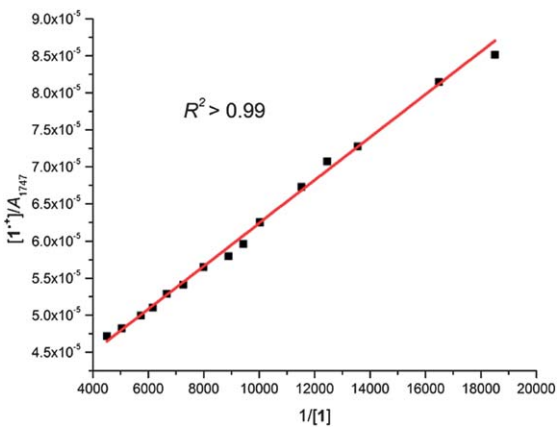

Fig. 4 Benesi–Hildebrand plot for dimeric $(\mathbf{1})_2^{+}$.

using the Gaussian 09 package.[69] Previous X-ray crystal structure analysis[34] and theoretical results unequivocally prove the benzenoid character of closed-shell **1**. In contrast, DFT analysis of $\mathbf{1}^+$ provides evidence for a delocalized[70] quinoidal structure (Fig. 5). This quinoidal nature is evident in the shortening of C_{ipso}–C_{ipso} bonds (*a*) by 1.5 pm and the C_{ortho}–C_{ortho} bonds (*c*) by 0.7 pm, as well as the elongation of the C_{ispo}–C_{ortho} bonds (*b*) by 0.6 pm. Interestingly, the arene rings in neutral **1** are non-uniformly canted to various degrees, ranging from 15° to 33°. In contrast, the benzene rings in $\mathbf{1}^+$ all flatten to a uniform torsional angle of 23° (Table 1).

Table 1 Theoretical[a] bond lengths (pm) and torsional angles (°)[b] of **1** and $\mathbf{1}^+$

Parameter	**1**	$\mathbf{1}^+$
a	148.7(1)	147.2(0)
b	140.8(1)	141.4(2)
c	139.1(2)	138.4(0)
θ	26(7)	23(0)

[a] DFT calculations performed at the RB3LYP/6-31G(d,p) or UB3LYP/6-31G(d,p) level of theory for **1** and $\mathbf{1}^+$, respectively. [b] Bond lengths are an average of symmetrically equivalent bonds; torsional angles are an average of symmetrically equivalent four-atom angles (*vide supra*, Fig. 5).

TD-DFT calculations for $\mathbf{1}^+$

In order to probe the origins of the optical transitions of $\mathbf{1}^+$, time-dependent (TD) DFT calculations were performed at the UB3LYP/6-31G(d,p) level of theory (Fig. 6 and Table S3 in the ESI†). Consistent with our experimental data, these calculations predict an absorption in the near-IR at 1414 nm ($f = 0.2601$) and in the visible region at 644 nm ($f = 0.0021$). The lower energy A-type[71] transition corresponds to a mixture of degenerate SOMO−1 β → SOMO β and SOMO−2 β → SOMO β, while the higher energy transition corresponds to a mixture of SOMO−5 β → SOMO β and SOMO−6 β → SOMO β. As a comparison, the sole predicted absorption for **1** at 340 nm ($f = 1.4872, 1.3057$) at the same level of theory involves the combination of HOMO−1 → LUMO, HOMO → LUMO+1, HOMO−2 → LUMO and HOMO → LUMO+2.[72] The small, broad shoulder around 400 nm present in neutral **1** arises from the symmetry-forbidden HOMO → LUMO transition.[38] Of particular significance is the decreased HOMO–LUMO gap (1.1 eV) for $\mathbf{1}^+$ compared to that of neutral **1** (3.2 eV).

Additionally, the frontier molecular orbitals encompassing these transitions (Fig. 6) were analyzed to further understand the electronic nature of $\mathbf{1}^+$. The occupied β orbitals involved show increased electron density along the C_{ipso}–C_{ipso} and C_{ipso}–C_{ortho} bonds, further confirming a delocalized quinoidal character. This electron distribution is also in good agreement with the shortened C_{ipso}–C_{ipso} (*a*) and C_{ortho}–C_{ortho} (*c*) bonds, as well as the lengthened C_{ipso}–C_{ortho} (*b*) bonds observed in the DFT optimized geometry (*vide supra*, Table 1).

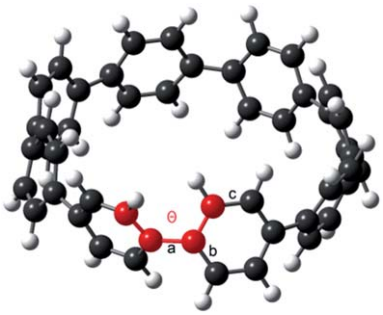

Fig. 5 DFT optimized geometry of $\mathbf{1}^+$ performed at the UB3LYP/6-31G(d,p) level of theory. Labels refer to the C_{ipso}–C_{ipso} (*a*), C_{ispo}–C_{ortho} (*b*) and C_{ortho}–C_{ortho} (*c*) bonds. The torsional angle (*θ*) between aryl rings is depicted in red.

DFT analysis of charge-resonance dimer $(\mathbf{1})_2^+$

In order to gain further insight into the interactions that contribute to the high stability of $(\mathbf{1})_2^+$, DFT calculations were performed at the UωB97X-D/6-31G(d,p)[74,75] level of theory in the gas phase. TD-DFT calculations on the optimized geometry at the same level of theory are consistent with the experimentally observed broad charge-resonance band in the NIR (Table S4 in the ESI†). In the optimized geometry (Fig. 7),[76] we observe a π → π* interaction between a significantly shortened C_{ipso}–C_{ipso} bond of one quinoidal nanohoop and the face of an aryl ring on the adjacent nanohoop 3.10 Å away. The donating C_{ipso}–C_{ipso} bond has shortened to 144.5 pm, while the torsional angle of this specific C_{ipso}–C_{ipso} bond further decreased to 13°. These structural deformations may contribute to the enhanced interaction in the nanohoop charge-resonance dimer.

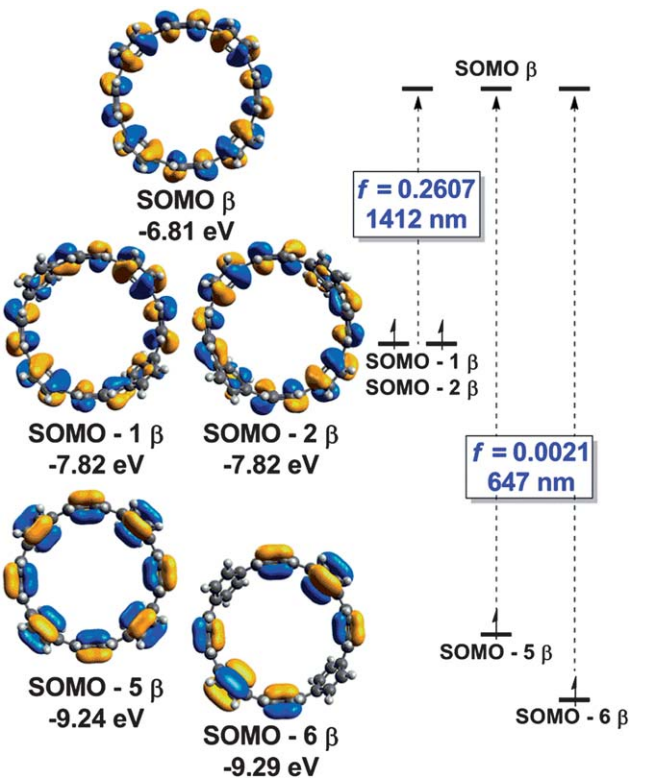

Fig. 6 Electronic transitions (TD-DFT) calculated at the UB3LYP/6-31G(d,p) level of theory with associated frontier molecular orbitals.[73]

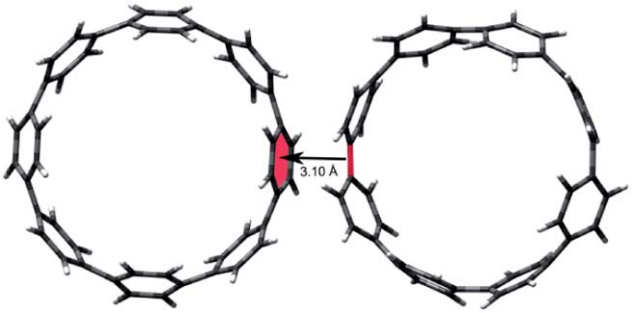

Fig. 7 Optimized geometry of $(\mathbf{1})_2^{\bullet+}$ at the UωB97X-D/6-31G(d,p) level of theory (gas phase) depicting the $\pi \rightarrow \pi^*$ interaction (highlighted in red).

We also computationally investigated the charge-resonance dimers arising from $([6]CPP)^{\bullet+}$, $([10]CPP)^{\bullet+}$ and $([12]CPP)^{\bullet+}$ to explore the relationship between [*n*]CPP size and binding strength. The geometries of the four nanohoop charge-resonance complexes were optimized after choosing a consistent set of Euler angles to orient one CPP ring relative to the other. This configuration was held constant in all four of the radical cation dimers. The restriction provided a consistent set of geometries for different sized [*n*]CPP charge-resonance dimers for comparison.

The binding energies were determined by subtracting the energies of two individual components (*i.e.* **1** and $\mathbf{1}^{\bullet+}$) from the energy of a dimeric structure (*i.e.* $(\mathbf{1})_2^{\bullet+}$) (Fig. 8).[77] From these data, a general trend emerges relating the size of the nanohoops in a charge-resonance dimer to the binding energy. Specifically, as the nanohoops become larger, the binding energy increases. Presumably, the positive charge is more delocalized throughout the quinoidal π-system in the larger nanohoops than in the smaller nanohoops, giving rise to the observed trend.

To begin investigating this trend experimentally, we attempted to characterize the charge-resonance complex of [12]CPP using the Benesi–Hildebrand procedure. However, even upon treating [12]CPP with a large excess of oxidant (20 equivalents) and prolonging the reaction time, we were never able to isolate or observe $[12]CPP^{\bullet+}$. Rather, only the paramagnetic charge-resonance complex $([12]CPP)_2^{\bullet+}$ was detected (Fig. S12 in the ESI†). Both the charge-resonance band in the NIR and the band in the visible region increased in intensity upon addition of neutral [12]CPP (Fig. S11 in the ESI†). These experimentally observed absorptions are consistent with the bands observed for $(\mathbf{1})_2^{\bullet+}$. Since $[12]CPP^{\bullet+}$ was not detectable under our experimental conditions, we were not able to measure the exact binding constant for this larger cycloparaphenylene. The experimental observation, however, is consistent with larger carbon nanohoops forming stronger charge-resonance dimers.

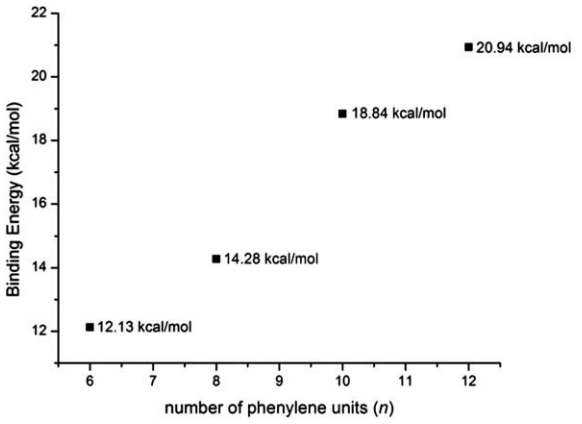

Fig. 8 Theoretical binding energies of [*n*]CPP charge-resonance dimers ($n = 6, 8, 10, 12$) calculated at the UωB97X-D/6-31G(d,p) level of theory (gas phase).

The study of intermolecular charge transfer in cycloparaphenylenes may have implications in analogous phenomena in single-walled CNTs. Prior theoretical[78] and experimental work on systems consisting of two crossed nanotubes has showed that metal–metal nanotube junctions have a very high conductance (0.1–0.2 e^2/h).[79–81] In addition, studies have shown a relationship between diameter and conductance in networks made exclusively of CNT bundles.[82] To our knowledge, however, there has been no single study explicitly relating CNT diameter and conductance across CNT–CNT junctions. Based on our results comparing differing sized [*n*]CPP charge-resonance dimers, carbon nanotube diameter should dramatically affect hole transport across intermolecular CNT junctions.

Conclusion

In summary, [8]CPP **1** was successfully chemically oxidized for the first time and isolated as a cationic hexachloroantimonate salt. A thorough comparison of bond lengths and angles derived *via* DFT calculations illustrates the delocalized quinoidal character of $\mathbf{1}^{\bullet+}$. The optical properties of this novel radical cation were further explored, displaying transitions in both the visible region and in the near-IR. TD-DFT calculations and an FMO analysis allowed us to relate the quinoidal structural data with the observed optical transitions, revealing four A-type transitions from singly-occupied β orbitals with varying quinoid-like character. The spectroscopic properties of $\mathbf{1}^{\bullet+}$ were then exploited to observe an *in situ* CR dimer with an unusually large binding constant, K_{dimer}. The charge-resonance band at 1747 nm was characteristic of extensive charge delocalization throughout both cycloparaphenylene rings. Furthermore, DFT calculations showed that a general trend exists relating nanohoop size and charge-resonance binding strength. The highly delocalized nature of the [*n*]CPP radical cations—both intramolecularly and intermolecularly—bodes well for their use in advanced organic electronics and photovoltaic devices.

Acknowledgements

Financial support was provided by the National Science Foundation (CHE-1255219) and generous startup funds from Boston University. The authors gratefully acknowledge Dr Jianlong Xia (Columbia University) and Prof. Robin G. Hicks (University of Victoria) for helpful discussions, Dr Sébastien Rochat (Massachusetts Institute of Technology) for assistance with spectroelectrochemical measurements, Mr Evan R. Darzi for

experimental assistance, Dr Jeffrey W. Bacon (Boston University) for assistance with X-ray crystallography, Dr Paul Ralifo and Dr Mekhala Pati (Boston University) for assistance with EPR spectroscopy, Prof. John Caradonna for the use of a glovebox and Prof. Linda Doerrer for the use of a UV-vis-NIR spectrophotometer. EPR facilities are supported by the National Science Foundation (CHE-0840418).

Notes and references

1 I. C. Lewis and L. S. Singer, *J. Chem. Phys.*, 1965, **43**, 2712–2727.
2 B. Badger and B. Brocklehurst, *Nature*, 1968, **219**, 263.
3 L. L. Miller and K. R. Mann, *Acc. Chem. Res.*, 1996, **29**, 417–423.
4 P. A. Sullivan and L. R. Dalton, *Acc. Chem. Res.*, 2009, **43**, 10–18.
5 M. Baumgarten and K. Müllen, *Top. Curr. Chem.*, 1994, **169**, 1–103.
6 K. Y. Law, *Chem. Rev.*, 1993, **93**, 449–486.
7 S. L. Hellstrom, M. Vosgueritchian, R. M. Stoltenberg, I. Irfan, M. Hammock, Y. B. Wang, C. Jia, X. Guo, Y. Gao and Z. Bao, *Nano Lett.*, 2012, **12**, 3574–3580.
8 B. Chandra, A. Afzali, N. Khare, M. M. El-Ashry and G. S. Tulevski, *Chem. Mater.*, 2010, **22**, 5179–5183.
9 R. G. Hicks, *Org. Biomol. Chem.*, 2007, **5**, 1321–1338.
10 R. Rathore and J. K. Kochi, *J. Org. Chem.*, 1995, **60**, 4399–4411.
11 R. Rathore, A. S. Kumar, S. V. Lindeman and J. K. Kochi, *J. Org. Chem.*, 1998, **63**, 5847–5856.
12 R. Rathore, C. L. Burns and M. I. Deselnicu, *Org. Lett.*, 2001, **3**, 2887–2890.
13 R. Rathore and C. L. Burns, *J. Org. Chem.*, 2003, **68**, 4071–4074.
14 R. Rathore, C. L. Burns and S. Abdelwahed, *Org. Lett.*, 2004, **6**, 1689–1692.
15 M. Banerjee, S. Lindeman and R. Rathore, *J. Am. Chem. Soc.*, 2007, **129**, 8070–8071.
16 J. Ferraris, D. O. Cowan, V. Walatka and J. H. Perlstein, *J. Am. Chem. Soc.*, 1973, **95**, 948–949.
17 M. Yoshizawa, K. Kumazawa and M. Fujita, *J. Am. Chem. Soc.*, 2005, **127**, 13456–13457.
18 I. Aprahamian, J.-C. Olsen, A. Trabolsi and J. F. Stoddart, *Chem.–Eur. J.*, 2008, **14**, 3889–3895.
19 M. Hasegawa, K. Daigoku, K. Hashimoto, H. Nishikawa and M. Iyoda, *Bull. Chem. Soc. Jpn.*, 2012, **85**, 51–60.
20 D. D. Graf, J. P. Campbell, L. L. Miller and K. R. Mann, *J. Am. Chem. Soc.*, 1996, **118**, 5480–5481.
21 D. D. Graf, R. G. Duan, J. P. Campbell, L. L. Miller and K. R. Mann, *J. Am. Chem. Soc.*, 1997, **119**, 5888–5899.
22 R. Takita, C. Song and T. M. Swager, *Org. Lett.*, 2008, **10**, 5003–5005.
23 R. Shomura, K. Sugiyasu, T. Yasuda, A. Sato and M. Takeuchi, *Macromolecules*, 2012, **45**, 3759–3771.
24 J. Janata, J. Gendell, C.-Y. Ling, W. E. Barth, L. Backes, H. B. Mark and R. G. Lawton, *J. Am. Chem. Soc.*, 1967, **89**, 3056–3058.
25 Y. Morita, S. Suzuki, K. Sato and T. Takui, *Nat. Chem.*, 2011, **3**, 197–204.
26 R. M. Dessau, S. Shih and E. I. Heiba, *J. Am. Chem. Soc.*, 1970, **92**, 412–413.
27 H. Becker, G. Javahery, S. Petrie, P. C. Cheng, H. Schwarz, L. T. Scott and D. K. Bohme, *J. Am. Chem. Soc.*, 1993, **115**, 11636–11637.
28 M. Baumgarten, L. Gherghel, M. Wagner, A. Weitz, M. Rabinovitz, P.-C. Cheng and L. T. Scott, *J. Am. Chem. Soc.*, 1995, **117**, 6254–6257.
29 H. A. Galue, C. A. Rice, J. D. Steill and J. Oomens, *J. Chem. Phys.*, 2011, **134**, 054310–054311.
30 P. J. Krusic, E. Wasserman, P. N. Keizer, J. R. Morton and K. F. Preston, *Science*, 1991, **254**, 1183–1185.
31 Y. Morita, A. Ueda, S. Nishida, K. Fukui, T. Ise, D. Shiomi, K. Sato, T. Takui and K. Nakasuji, *Angew. Chem., Int. Ed.*, 2008, **47**, 2035–2038.
32 H. Rath, S. Tokuji, N. Aratani, K. Furukawa, J. M. Lim, D. Kim, H. Shinokubo and A. Osuka, *Angew. Chem., Int. Ed.*, 2010, **49**, 1489–1491.
33 R. Jasti, J. Chattacharjee, J. B. Neaton and C. R. Bertozzi, *J. Am. Chem. Soc.*, 2008, **130**, 17646–17647.
34 J. Xia, J. W. Bacon and R. Jasti, *Chem. Sci.*, 2012, **3**, 3018–3021.
35 H. Takaba, H. Omachi, Y. Yamamoto, J. Bouffard and K. Itami, *Angew. Chem., Int. Ed.*, 2009, **48**, 6112–6116.
36 Y. Ishii, Y. Nakanishi, H. Omachi, S. Matsuura, K. Matsui, H. Shinohara, Y. Segawa and K. Itami, *Chem. Sci.*, 2012, **3**, 2340–2345.
37 S. Yamago, Y. Watanabe and T. Iwamoto, *Angew. Chem., Int. Ed.*, 2010, **49**, 757–759.
38 T. Iwamoto, Y. Watanabe, Y. Sakamoto, T. Suzuki and S. Yamago, *J. Am. Chem. Soc.*, 2011, **133**, 8354–8361.
39 S. Hitosugi, W. Nakanishi, T. Yamasaki and H. Isobe, *Nat. Commun.*, 2011, **2**, 492.
40 T. Nishiuchi, X. Feng, V. Enkelmann, M. Wagner and K. Müllen, *Chem.–Eur. J.*, 2012, **18**, 16621–16625.
41 R. Jasti and C. R. Bertozzi, *Chem. Phys. Lett.*, 2010, **494**, 1–7.
42 E. S. Hirst and R. Jasti, *J. Org. Chem.*, 2012, **77**, 10473–10478.
43 H. Omachi, Y. Segawa and K. Itami, *Acc. Chem. Res.*, 2012, **45**, 1378–1389.
44 T. Iwamoto, Y. Watanabe, T. Sadahiro, T. Haino and S. Yamago, *Angew. Chem., Int. Ed.*, 2011, **50**, 8342–8344.
45 We refer to the [*n*]cycloparaphenylenes as carbon nanohoops because they are the smallest possible fragment of an [*n*,*n*] armchair carbon nanotube.
46 A. V. F. Zabula, A. S. Filatov, J. Xia, R. Jasti and M. A. Petrukhina, *Angew. Chem., Int. Ed.*, 2013, **52**, 5033–5036.
47 For details on previous cyclic voltammetry measurements, see ref. 38 and 72
48 J. K. Kochi, R. Rathore and P. L. Maguères, *J. Org. Chem.*, 2000, **65**, 6826–6836.
49 J. Chen, C. Klinke, A. Afzali and P. Avouris, *Appl. Phys. Lett.*, 2005, **86**, 123108.
50 F. Marchetti, C. Pinzino, S. Zacchini and G. Pampaloni, *Angew. Chem., Int. Ed.*, 2010, **49**, 5268–5272.

51 X. Chen, X. Wang, Y. Sui, Y. Li, J. Ma, J. Zuo and X. Wang, *Angew. Chem., Int. Ed.*, 2012, **51**, 11878–11881.
52 T. S. Navale, K. Thakur, V. S. Vyas, S. H. Wadumethrige, R. Shukla, S. V. Lindeman and R. Rathore, *Langmuir*, 2012, **28**, 71–83.
53 P. H. Rieger, *Electron Spin Resonance: Analysis and Interpretation*, RSC Publishing, Cambridge, 2007.
54 M. Takase, T. Narita, W. Fujita, M. S. Asano, T. Nishinaga, H. Benten, K. Yoza and K. Müllen, *J. Am. Chem. Soc.*, 2013, **135**, 8031–8040.
55 Twinned crystals were obtained by slowly cooling the reaction mixture to −30 °C over the course of 7 days. Unfortunately, refinement of the crystal structure was unsuccessful. Since a stoichiometric amount of antimony trichloride by-product was present during crystallization it is likely that the $SbCl_6^-$ anion sites were partially occupied by disordered $SbCl_3$. The antimony trichloride could be removed by the purification procedure described in the ESI,† but attempts at crystallizing the purified compound under numerous conditions were unsuccessful.
56 H. Ueda, *Bull. Chem. Soc. Jpn.*, 1968, **41**, 2578–2586.
57 S. Mah, Y. Yamamoto and K. Hayashi, *J. Phys. Chem.*, 1983, **87**, 297–300.
58 C. Lin, T. Endo, M. Takase, M. Iyoda and T. Nishinaga, *J. Am. Chem. Soc.*, 2011, **133**, 11339–11350.
59 F. Zhang, G. Gotz, E. Mena-Osteritz, M. Weil, B. Sarkar, W. Kaim and P. Bauerle, *Chem. Sci.*, 2011, **2**, 781–784.
60 J. Rose, *Molecular Complexes*, Pergamon Press, New York, 1967.
61 H. A. Benesi and J. H. Hildebrand, *J. Am. Chem. Soc.*, 1949, **71**, 2703–2707.
62 M. A. J. Rodgers, *J. Chem. Soc., Faraday Trans. 1*, 1972, **68**, 1278–1286.
63 A. Ayalon, A. Sygula, P.-C. Cheng, M. Rabinovitz, P. W. Rabideau and L. T. Scott, *Science*, 1994, **265**, 1065–1067.
64 I. Aprahamian, D. Eisenberg, R. E. Hoffman, T. Sternfeld, Y. Matsuo, E. A. Jackson, E. Nakamura, L. T. Scott, T. Sheradsky and M. Rabinovitz, *J. Am. Chem. Soc.*, 2005, **127**, 9581–9587.
65 A. Zabula, A. Filatov, S. Spisak, A. Rogachev and M. Petrukhina, *Science*, 2011, **333**, 1008–1011.
66 A. V. Zabula, S. N. Spisak, A. S. Filatov and M. A. Petrukhina, *Organometallics*, 2012, **31**, 5541–5545.
67 As pointed out by an insightful reviewer, aggregates formed from a 1 : 1 ratio of **1** and $\mathbf{1}^+$ or "hoop-in-hoop" complexes could also lead to a high binding constant. Further studies are warranted to differentiate between these alternate hypotheses
68 For examples of analyzing aromatic radical cations with DFT calculations and aromatic compounds that undergo structural change upon oxidation to a radical cation, see: (*a*) H. Shorafa, D. Mollenhauer, B. Paulus and K. Seppelt, *Angew. Chem., Int. Ed.*, 2009, **48**, 5845; (*b*) X. Chen, X. Wang, Y. Sui, Y. Li, J. Ma, J. Zuo and X. Wang, *Angew. Chem., Int. Ed.*, 2012, **51**, 11878.
69 See ESI† for full citation: M. J. Frisch *et al.*, *Gaussian 09, Revision B.01*, Wallingford, CT, 2009.
70 See Fig. S5 in the ESI†
71 S. Nelsen, M. Weaver, D. Yamazaki, K. Komatsu, R. Rathore and T. Bally, *J. Phys. Chem. A*, 2007, **111**, 1667–1676.
72 J. Xia, M. R. Golder, M. E. Foster, B. M. Wong and R. Jasti, *J. Am. Chem. Soc.*, 2012, **134**, 19709–19715.
73 FMO images were generated using Avogadro: M. Hanwell, D. Curtis, D. Lonie, T. Vandermeersch, E. Zurek and G. Hutchison, *J. Cheminf.*, 2012, **4**, 17.
74 J.-D. Chai and M. Head-Gordon, *J. Chem. Phys.*, 2008, **128**, 084106–084115.
75 J.-D. Chai and M. Head-Gordon, *Phys. Chem. Chem. Phys.*, 2008, **10**, 6615–6620.
76 The ωB97X-D functional has been successfully shown to model charge-transfer complexes, despite the inherent difficulty in modeling their interaction energies with DFT calculations: N. S. Stephan, P. Cyril, D. Aurore and C. Clemence, *J. Chem. Theory Comput.*, 2012, **8**, 1629.
77 For additional details, see Table S3 in the ESI†
78 S. Dag, R. T. Senger and S. Ciraci, *Phys. Rev. B: Condens. Matter Mater. Phys.*, 2004, **70**, 205407.
79 M. S. Fuhrer, J. Nygård, L. Shih, M. Forero, Y.-G. Yoon, M. S. C. Mazzoni, H. J. Choi, J. Ihm, S. G. Louie, A. Zettl and P. L. McEuen, *Science*, 2000, **288**, 494–497.
80 V. Margulis and M. Pyataev, *Phys. Rev. B: Condens. Matter Mater. Phys.*, 2007, **76**, 085411–085417.
81 M. S. Fuhrer, A. K. L. Lim, L. Shih, U. Varadarajan, A. Zettl and P. L. McEuen, *Phys. E.*, 2000, **6**, 868–871.
82 D. Hecht, L. Hu and G. Gruner, *Appl. Phys. Lett.*, 2006, **89**, 133112–133113.